Magnetic Resonance Imaging 56 (2019) 126–130

Contents lists available at ScienceDirect

Magnetic Resonance Imaging

journal homepage: www.elsevier.com/locate/mri

Original contribution

Dynamics of ionic liquids in poly(vinyl alcohol) porous scaffold. Low field NMR study

Carlos Mattea*, Bulat Gizatullin, Siegfried Stapf

Institute of Physics FG Technische Physik II/Polymerphysik, Technische Universität Ilmenau, D-98684 Ilmenau, Germany

ARTICLE INFO

Keywords:
Polymer-porous media
Ionic liquids
Dynamics
Diffusion
Single sided NMR

ABSTRACT

In this study molecular dynamics of ionic liquids in poly(vinyl alcohol) scaffolds were investigated. The binary poly(vinyl alcohol) – ionic liquid (PVA-IL) compound was prepared from initial solutions of water, ionic liquid (IL) and poly(vinyl alcohol) (PVA) at different concentrations. Subsequently water was evaporated under open conditions, leaving the scaffold/IL system of interest. Low field nuclear magnetic resonance (NMR) relaxation and diffusion measurements, as well as 2D T_1-T_2 correlated NMR experiments were performed to determine specific local and translational dynamics properties at different time scales. Data suggest that during water evaporation, partial demixing of IL from the polymeric matrix leaves the remaining solvent confined in the porous structure formed by the PVA polymer. The results show that the translational diffusion, as well as the local rotational molecular dynamics is comparable to the bulk liquid state. Moreover, in partial saturation conditions, diffusion shows enhancements relative to the bulk.

1. Introduction

Poly(vinyl alcohol) (PVA) is a well-known hydrophilic polymer with biocompatibility properties. PVA-derived porous media find applications commonly in biomedical and food industry. Mixed with certain solvents and water, it has been used for preparations of hydrogels [1]. PVA is a suitable material for developing scaffolds with a three-dimensional interconnected porous structure with a variety of architectural configurations [2]. This structure is usually achieved by repeated freeze–thawing cycles, which induces hydrogen bonding (physical cross-links), crystallization, and phase separation. The presence of microcrystals in these PVA scaffolds displays high mechanical strength and stiffness [3,4]. Other techniques to develop PVA scaffolds include solvent casting-particulate leaching [5], melt molding [6] and thermal induced phase separation [7]. Cross-linking can be as well induced via chemical agents and by use of γ-irradiation [8]. However, the fabrication of PVA structures combining high porosity, controllable pore morphology, and adequate mechanical properties for specific applications remains a challenge. Regarding electrochemical applications, pure PVA does not possess protonic conductivity, unless organic functional groups are added (sulfonate, hydroxyl, carboxylate, amine, phenolic). Considering the contemporary interest of ionic liquids [10] in the field of energy storage and release, the combination of PVA with ILs can be used for the purpose of adding ionic conductivity in these compounds. IL combined with polymers form different structures depending on concentration and nature of ions [11]. In materials called ionogels [12], IL are hybridized with another organic or inorganic components like low molecular weight gelators, (bio)polymers, carbon nanotubes or silica, in order to form hybrid materials where the IL is kept confined, acting as structuring media. In this case, the IL is taking place in the intrinsic organization of these materials, influencing the building of the solid host network and affecting their physicochemical properties [12,13]. Ionogels are used in electrolyte membranes, optical devices, catalysts and sensors. Apart from the cases where immobilization of the ions in the wall of the porous materials can make them more suitable for specific applications [15], there are many topics where the (translational) mobility of ions under confinement is required. A number of reports are related with the study of dynamics if ILs confined in materials like silica nanopores [9,15], biopolymers like gelatin [17], carbon nanotubes [18] and membranes [19].

The knowledge of the dynamical characteristics of the solvent IL inside the polymeric or inorganic silica porous matrix together with its pore structure becomes crucial in order to determine whether one can extend the application field of these compounds to electrodes, batteries, capacitors [14] or as a tailored biocompatible porous medium, even in the case when IL is removed. It is well known that thermodynamic properties such as melting point and glass transition temperatures are modified when liquids are under geometrical restrictions [15]. Normal

* Corresponding author.
E-mail address: carlos.mattea@tu-ilmenau.de (C. Mattea).

https://doi.org/10.1016/j.mri.2018.09.032
Received 31 August 2018; Accepted 26 September 2018

liquids under confinement exhibit, in general, restricted dynamics when compared to the bulk due to constraints in space at sufficient small poresize, and due to physico-chemical interactions between IL molecules and the surface of the pore walls [33] (i.e. absorption-desorption processes). However, in the case of ILs the situation becomes more complex, for instance demonstrated by the finding of enhanced diffusive mobility of confined IL [9,14,18–21].

Nuclear Magnetic Resonance (NMR) provides a suitable non-invasive experimental access to confined fluids. It allows the determination of diffusion coefficients related with intermolecular dynamics, and characteristic relaxation times related to local rotational dynamics. In particular, NMR diffusion in porous media uses the fluid molecules as tracers providing the pore space of the material of interest. This allows the determination of surface-to-volume ratios, average pore sizes or connectivity.

In the present work porous structures are prepared combining PVA with ILs. The samples are rigid non-transparent films (see below). The IL remains confined inside the PVA scaffold retaining its fluid character. The structure of the samples is further characterized using X-ray diffractometry and scanning electron microscopy. NMR is used in this setting to gain dynamic information on the ILs molecules, as well as to determine their averaged pore size.

The interest of the authors in this work focused on characterizing the interaction type between IL molecules and PVA and its influence on (i) the dynamics of the confined liquid and (ii) the structural morphology of the entire sample. Additionally, the possibility to remove the host IL and retain only the pure PVA-porous scaffold will be addressed.

2. Materials and methods

PVA (average molecular weight 67 kg/mol), acetone with a purity of > 99.7%, and the room temperature ionic liquids 1-ethyl-3-methylimidazolium-bis(trifluoromethylsulfonyl)imide ($EMIM^+$ $Tf2N^-$), (M_w = 391.31 g/mol and density 1.52 g cm^{-3} @ 293.15 K), 1-butyl-3-methylimidazolium - tetrafluoroborate ($EMIM^+$ $BF4^-$), (M_w = 226.02 g/mol and density 1.21 g cm^{-3} @ 293.15 K), all with a purity of > 97%, were purchased from Sigma Aldrich, Germany. All chemicals were used without further purification. Distilled water was used in all the preparations.

The preparation of the samples is performed as follows: a mixture of a predetermined volume of IL with water was heated to 80 °C using a magnetic stirrer, followed by the addition of a defined quantity of PVA in order to obtain the desired concentration of PVA and IL. The procedure is based on previous preparations of film consisting of PVA in water, from reference [16], and films of ILs in gelatin, from reference [17]. The mixture was stirred at the same temperature until the polymer was completely solubilized. The solution was then cast onto a Petri dish of 65 mm diameter and kept at ambient temperature and humidity (20 °C, RH around 46% within 5%). In these conditions the water was allowed to evaporate until the samples were formed and no further weight loss was observed. The height of the samples was typically 1 mm. Due to their negligible vapor pressure, the ionic liquids remained within the polymer. The amount of water in the initial solution is approximately the same as the IL. The exact amount of water is not critical because water is used to help in the dissolution of PVA. The water content in each final sample was < 3%, determined by comparing the weight of the samples before and after oven drying at 100 °C, under vacuum of 5 mbar, over 24 h. All samples were measured several days after preparation. The description of the relative component of IL and polymer is found in Table 1, where a label was given to each sample. Sample 3-U and Sample 4-U (U for “unsaturated”) are obtained from Sample 3 and Sample 4, respectively, by dilution of the IL with acetone after the following protocol: around 0.5 g of each sample was imbibed in 5 ml of acetone and kept in a closed vial at room temperature under stirring for > 48 h. No visible degradation was observed. The samples were then dried under vacuum (~5 mbar) overnight at 60 °C.

Table 1
Sample description with the relative proportion of IL and PVA. The saturation indicates the percentage of IL that fills the pores in each sample.

Name	Emim Tf2N:PVA	Bmim BF4:PVA	Saturation
Sample 1	2:1	–	100%
Sample 2	1:2	–	100%
Sample 3	1.5:1	–	100%
Sample 3-U	1.5:1	–	Approx. 40%
Sample 4	–	1:1	100%
Sample 4-U	–	1:1	Approx. 50%

A single-sided NMR scanner (NMR MOUSE, Magritek, Germany) with a sensor providing a sensitive circular area of about 75 mm^2 was employed for the NMR diffusion measurements. The MOUSE device [31] is operated at a ^{1}H Larmor frequency of 18.7 MHz, and possesses a static magnetic field gradient of 21.6 T/m. It has an accessible vertical range of 3.0 mm. The digital resolution is determined by the combination of the spectral width, acquisition time, and gradient strength [22,31]. The minimum 180° pulse separation (*TE*) is determined by the acquisition time of the echo preceded and followed by the dead-time of the system. The echo time (TE) was 52 μs and the dead-time of the system is in the order of 20 μs. The Carr − Purcell − Meiboom − Gill (CPMG) pulse sequence [28,29] is applied in the NMR MOUSE device to accumulate T_2-weighted echo trains after the usual diffusion and spin-lattice relaxation time pulse sequences in order to increase sensitivity [31]. As explained in detail in reference [17], due to the strong gradient and frequency of excitation, both ^{1}H and ^{19}F nuclei fulfill the condition $\omega = \gamma B_0$ inside the field of view of the scanner, above the radio-frequency (RF) coil, allowing a selection of either ^{1}H or ^{19}F when the thickness of the film is less than the distance between the location of ^{1}H and ^{19}F resonances. The magnet in the single-sided NMR scanner is mounted on a lift, allowing the acquisition of vertical profiles moving the scanner relative to the sample [17,31]. In the present work, the vertical profiles were used only to locate the middle of the samples and select the nucleus of interest. The 90° RF pulse length was set to 4.75 μs. The diffusion measurements were carried out using the stimulated echo pulse sequence [22,30] $\left(\pi/2 \ldots \tau \ldots \pi/2 \ldots \Delta \ldots cpmg\right)$, combined with the constant gradient of the device. $\left(\pi/2\right)$ represents the 90° pulses, Δ is the diffusion time and τ the encoding time. All the echoes after the third 90° pulse are integrated to increase sensitivity.

2D T_1-T_2 correlated NMR experiments were run in a low-field spectrometer (Spinsolve, Magritek, Germany) working at ^{1}H Larmor frequency of 43 MHz. The inversion recovery [22] pulse sequence was used for T_1 determination using a CPMG pulse sequence as acquisition, for every recovery time in combination with FID acquisition between the second 90° pulse and the first 180° pulse of the cpmg train. The data were recorded in a 2 dimensional matrix and inverted [23]. The temperature of the sample in this spectrometer is 27 °C.

X-ray diffraction (XRD) measurements, a Philips X'Pert PRO diffractometer, equipped with a wide-range PW 3050/6× goniometer capable to measure 0.001°/step was used. The XRD pattern were obtained at room temperature using Cu K-α radiation (λ = 0.154 nm) generated at a voltage of 35 kV and 30 mA current. The sample was scanned between 2θ = 1.5 to 60° with a step size of 0.050°, scanning speed of 2°/min and a count time of 100 s per point.

For analyzing the effect of the ILs on the polymer microstructure, scanning electron microscope (SEM) images were obtained with a Hitachi S218 4800 II.

3. Results and discussion

The microstructure of the PVA matrix was studied using X-ray and electron microscopy. Fig. 1 shows the X-ray diffraction profile of

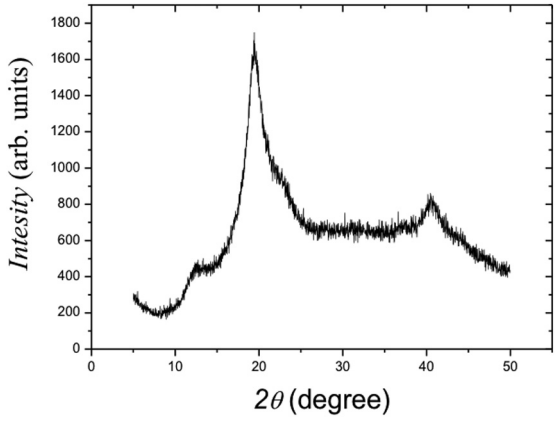

Fig. 1. X-ray pattern of the Sample 1.

Sample 1. The pattern is characteristic of the pure PVA solid polymer as can be found in literature [3]. The X-ray diffraction profile is practically independent of the concentration if IL used in the different samples in this work. This provides an evidence that IL inside the porous matrix is not altering the microstructure of the pure PVA, as in the case of a rigid gel, or in so-called ionogels. As has been shown in literature listed in the Introduction section, porous structures can be created from pure PVA hydrogels after leaching of water. It becomes evident that the IL remaining in the samples listed in Table 1, is hosted inside the solid PVA in a kind of porous structure. This study aims at possibilities to probe this statement and to quantify the molecular mobility of IL under confinement.

The structure of the samples can be further explored by using electron microscopy. Fig. 2 shows the SEM images of Emim-Tf2N in solid PVA (Sample 1) and Bmim-BF4 in solid PVA (Sample 4), respectively. A porous microstructure is observed with pore sizes in the order of few micrometers, but still little can be said about interconnectivity of porous voids. SEM images are not able to provide precise information about pore sizes in the samples that are smaller than few micrometers. NMR can extend the range of estimation of pore sizes, through measurements of relaxation times and diffusion of the IL molecules confined in the PVA matrix, is used to estimate the pore dimensions of the samples.

^{1}H NMR relaxation times were measured in Sample 1 which corresponds to EmimTFSI in PVA in the proportion 2:1 (see Table 1). The T_1-T_2 correlation maps showing the separate ^{1}H relaxation values corresponding to both the liquid and confining matrix are presented in Fig. 3a. Similar measurements were performed in a pure PVA sample prepared following the same protocol as the sample in Table 1, without including any IL (Fig. 3b). The low T_2 relaxation values correspond to the solid PVA porous matrix, with a broad distribution of T_1 relaxation times centered around 700 ms corresponding to the amorphous region of the solid matrix. The long T_1 component is related to the crystalline PVA. Interestingly, no major changes are observed in the solid polymeric matrix component in Sample 1, except a small decreasing in the long T_2 component of the crystalline part. The long component values of T_2 and T_1 in the diagonal correspond to the confined IL and are identical, within experimental errors, to the bulk values [27]. This experiment shows that the discrimination of the IL and solid PVA components is possible because of the T_2 encoding, but cannot be resolved from a pure T_1 experiment.

The determination of the diffusion values was carried out for all the samples described in Table 1. The different ions of the ILs studied in this work can be encoded separately in an NMR experiment because they contain ^{1}H nuclei only in the cations and ^{19}F nuclei only in the anions. As explained in Section 2 and in reference [17], the single sided NMR scanner is able to measure these nuclei separately, provided that the sample has a thickness below the distance between the two corresponding ^{1}H and ^{19}F resonances above the surface of the radio-frequency coil in the device (~1.3 mm). This condition is fulfilled in all the samples listed in Table 1.

Fig. 4 shows the results of the diffusion experiment performed on Samples 1 and 2. The diffusion constants were measured at different observation times (Δ). The difference in the diffusivity between the cations and anions is well known and reported in literature [32]. The values of diffusion at short Δ times are identical to the bulk IL in both samples. This result, in agreement with the findings of the relaxation experiments above, confirm that translational and local rotational dynamics are not affected by the confinement. However at longer observation times, the samples prepared with different proportion of IL and PVA, have different influence in the translational diffusion due to the different confining properties. Using the fact that at short diffusion times $D(t)$ provides information about the surface-to-volume ratio, an estimation of the pore size can be obtained assuming spherical pore shape, from the equation [24,25].

$$D(\Delta) = D_0\left(1 - \frac{4}{9}\frac{S}{V}\sqrt{D_0\Delta/\pi}\right), \quad (1)$$

where S/V is the surface to volume ratio and D_0 the bulk diffusion of the

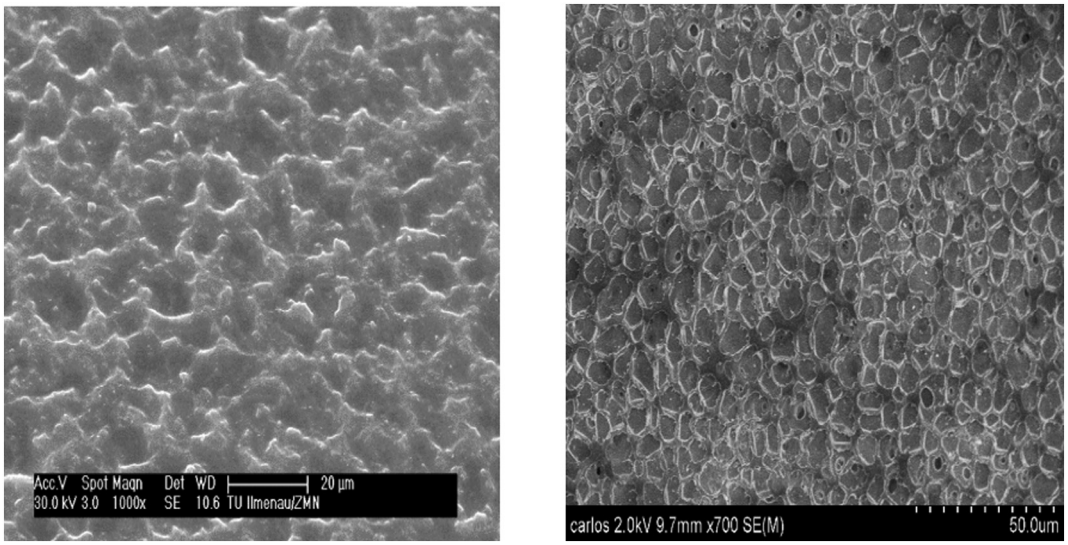

Fig. 2. SEM images of Sample 1 (left) and Sample 4 (right).

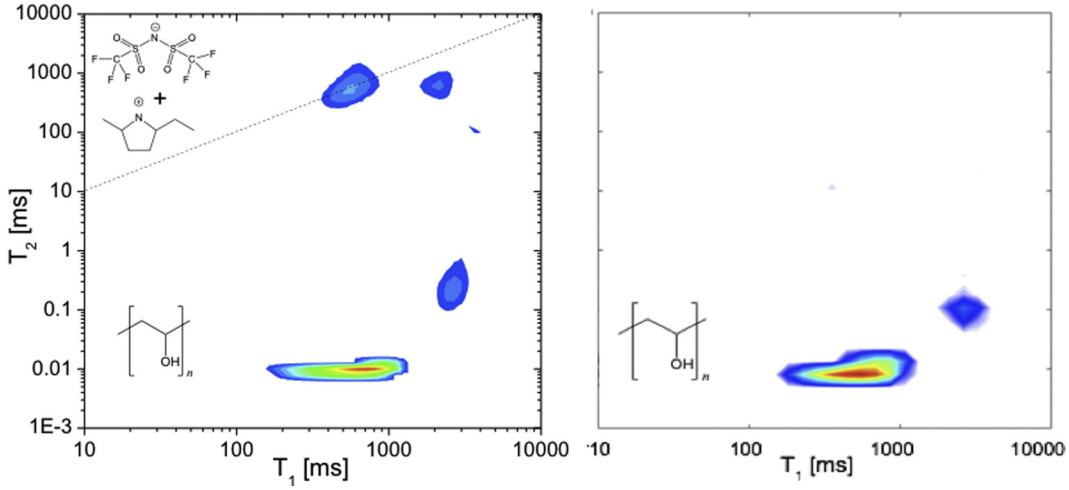

Fig. 3. ^{1}H T_1-T_2 correlation maps of Emim Tf2N in PVA scaffold (Sample 1, left) showing the decoupled relaxation values corresponding to the liquid and the confining matrix, respectively. The diagonal indicates the values corresponding to $T_1 = T_2$. The right panel shows the pure PVA matrix without IL. The ^{1}H T_1 relaxation time of the Emim Tf2N in bulk at 27 °C is (420 ± 30) ms.

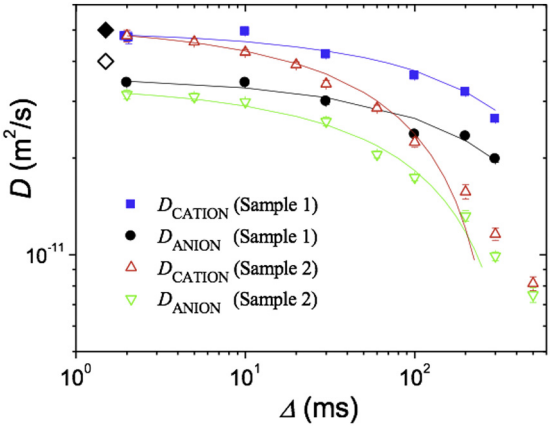

Fig. 4. Diffusion constants of cations and anions of EmimTf2N in two different PVA scaffolds: Sample 1, solid symbols and Sample 2, open symbols). Δ is the diffusion time. The lines correspond to the model in Eq. (1). The bulk IL diffusion values are indicated as diamond symbols (solid and open corresponds to cation and anion, respectively).

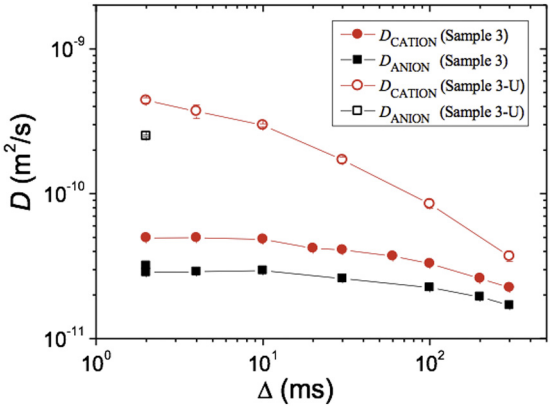

Fig. 5. Diffusion constants of cations and anions of EmimTf2N in saturated Sample 3 (solid symbols) and unsaturated Sample 3-U (open symbols).

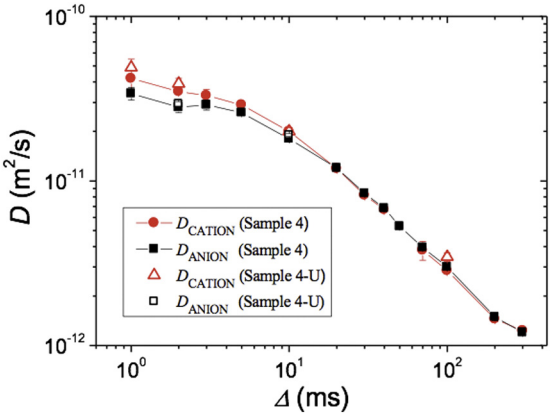

Fig. 6. Diffusion constants of cations and anions of Bmim BF4 in saturated Sample 4 (solid symbols) and unsaturated Sample 4-U (open symbols).

confined species.

By fitting the experimental data using Eq. (1), from the surface to volume ratio, average pore sizes of 3 μm and 6 μm were derived (samples 1 and 2, respectively). This result shows that by varying the proportion of IL and PVA, one is able to tune certain geometrical properties of these hybrid materials.

In a second step, the possibility to fabricate porous materials from the IL-PVA samples, without IL, with specific structural properties or specific functionalized surfaces was explored. This procedure further allows the study of dynamics of the solvents under two conditions: saturation and partial saturation. Therefore, an attempt to extract the IL, from Sample 3 and Sample 4, was made. Diffusion measurements were carried out in Sample 3, Sample 3-U, Sample 4 and Sample 4-U. The results are shown in Figs. 5 and 6. Diffusion is enhanced dramatically in the Sample 3-U containing the shorter alkyl chain in the cation combined with the anion Tf2N. A single measurement was done for determining the diffusion of the anion in the same sample, at Δ = 2 ms. The result is consistent with what was observed in the cations, showing as well a clear diffusion enhancement. In the sample where the IL Bmim BF4 was used, practically no enhancement in the diffusion values was observed. The echo decays obtained in the Sample 4-U during diffusion measurements were showing a small deviation from a single exponential decay.

The molecular mechanisms underlying the increasing in the translational dynamics in Sample 3-U are not yet clear. In other systems, like water and some organic solvents in unsaturated glass-porous media, diffusion is enhanced [34,35] due to the presence of the vapor phase of the same liquid inside the porous, allowing the molecules to escape from the liquid wetting the pore-walls and make excursion into the

vapor phase. However, the negligible vapor pressure of the ILs hinders such mechanism.

The nature of the intermolecular interaction may play a role in the explanation of the phenomena. Apart of the coulombic electrostatic interaction, the ILs under study in this work form hydrogen bonded (HB) three dimensional networks [36,37]. HB depends on the intermolecular distance between the H-donor in the imidazolium ring and the Oxygen in the sulfonyl groups in the anion Tf2N and the Fluor in the BF4 anions, and the angle between the C…H bond and the acceptor atom. The HB interaction in the Bmim BF4 IL is stronger than the corresponding HB interaction in the Emim Tf2N IL [38]. When the IL content is reduced inside the pore, the effective three dimensional HB network may be disrupted in the case of Emim Tf2N, but remaining still effective in the case of Bmim BF4.

Fumino et al. [39], on the other hand, have reported that whereas molecular liquids are stabilized by hydrogen bonding, ionic liquids can instead be fluidized by hydrogen bonds. They have shown using FTIR spectroscopy that highly directional H B introduce “defects” into the Coulomb network resulting in reduced melting points and decreased viscosities. Whether this is the reason for the diffusion enhancement remains still not clear and further investigation is necessary in order to interpret the results.

4. Conclusions

Polymeric rigid porous matrix with pore size in the order of few micrometers, confining ionic liquids can be fabricated opening possibilities to tune pore size by setting the concentration and type of IL.

The samples are acting more as hosting solid matrices confining IL with bulk mobility, putting our materials on the other extreme of the so called ionogel hybrid materials.

Estimation of pore sizes could be performed using NMR diffusometry. The results are in agreement with SEM estimations.

In saturation NMR relaxation and diffusion show that bulk translational and rotational dynamics is retained at short diffusion times. The geometric restrictions appears at long diffusion times.

The unsaturated samples with ionic liquids containing the Tf2N anion exhibit enhanced dynamics relative to the bulk.

Acknowledgments

The authors thank Kerstin Geyer and Paul Denner for helping in the sample preparation and for X-Ray Diffraction measurements. Maximilian Kaupenjohann is acknowledged for sample preparation and discussions.

References

[1] Hyon S-H, Cha W-I, Ikada Y. Preparation of transparent poly(vinyl alcohol) hydrogel. Polym Bull 1989;22:119–22.
[2] Ye M, Mohanty P, Ghosh G. Morphology and properties of poly vinyl alcohol (PVA) scaffolds: impact of process variables. Mater Sci Eng C 2014;42:289–94.
[3] Gupta S, Webster T, Sinha A. Evolution of PVA gels prepared without crosslinking agents as a cell adhesive surface. J Mater Sci Mater Med 2011;22:1763–72.
[4] Hassan C, Peppas N. Structure and applications of poly(vinyl alcohol) hydrogels produced by conventional crosslinking or by freezing/thawing methods. Adv Polym Sci 2000;153:37–65.
[5] Sin D, Miao X, Liu G, Wei F, Chanwick G, Yan C, et al. Polyurethane (PU) scaffolds prepared by solvent casting/particulate leaching (SCPL) combined with centrifugation. Mater Sci Eng C 2010;30:78–85.
[6] Oh S, Kang S, Kim E, Cho S, Lee J. Fabrication and characterization of hydrophilic poly(lactic-co-glycolic acid)/poly(vinyl alcohol) blend cell scaffolds by melt-molding particulate-leaching method. Biomaterials 2003;24:4011–21.
[7] Kim J, Kim J, Lee Y, Drioli E. Thermally-induced phase separation (TIPS) and electrospinning methods for emerging membrane applications: a review. AICHE J 2016;62:461–90.
[8] Nikolic V, Krkljes A, Popovic Z, Lausevic Z, Miljanic S. On the use of gamma irradiation crosslinked PVA membranes in hydrogen fuel cells. Electrochem Commun 2007;9:2661–5.
[9] Garaga M, Aguilera L, Yaghini N, Matic A, Persson M, Martinelli A. Achieving enhanced ionic mobility in nanoporous silica by controlled surface interactions. Phys Chem Chem Phys 2017;19:5727–36.
[10] Welton T. Room-temperature ionic liquids. Solvents for synthesis and catalysis. Chem Rev 1999;99:2071–84.
[11] Yoon J, Lee H, Stafford C. Thermoplastic elastomers based on ionic liquid and poly (vinyl alcohol). Macromolecules 2011;44:2170–8.
[12] Le Bideau J, Viau L, Vioux A. Ionogels, ionic liquid based hybrid materials. Chem Soc Rev 2011;40:907–25.
[13] Singh M, Singh S, Chandra S. Ionic liquids confined in porous matrices: physicochemical properties and applications. Prog Mater Sci 2014;64:73–120.
[14] Pinilla C, Del Popolo M, Lynden-Bell R, Kohanoff J. Structure and dynamics of a confined ionic liquid. Topics of relevance to dye-sensitized solar cells. J Phys Chem B 2005;109:17922–7.
[15] Gupta AK, Verma YL, Singh RK, Chandra S. Studies on an ionic liquid confined in silica nanopores: change in Tg and evidence of organic-inorganic linkage at the pore wall surface. J Phys Chem C 2014;118:1530–9.
[16] Ghoshal S, Denner P, Stapf S, Mattea C. Study of the formation of poly(vinyl alcohol) films. Macromolecules 2012;45:1913–23.
[17] Mattea C, Ordikhani-Seyedlar A, de Almeida Silva P, Stapf S. Molecular transport in ionic liquids under confinement studied by low field NMR. Microporous Mesoporous Mater 2018;269:171–4.
[18] Ghoufi A, Szymczyk A, Malfreyt P. Ultrafast diffusion of ionic liquids confined in carbon nanotubes. Sci Rep 2016;6(28518):1–9.
[19] Thomaz J, Bailey H, Fayer M. The influence of mesoscopic confinement on the dynamics of imidazolium-based room temperature ionic liquids in polyether sulfone membranes. J Chem Phys 2017;147(194502):1–11.
[20] Filippov A, Gnezdilov O, Hjalmarsson N, Antzutkin O, Glavatskih S, Furó I, et al. Acceleration of diffusion in ethylammonium nitrate ionic liquid confined between parallel glass plates. Phys Chem Chem Phys 2017;19:25853–8.
[21] Chathoth S, et al. Fast diffusion in a room temperature ionic liquid confined in mesoporous carbon. Europhys Lett 2012;66004(1–6):97.
[22] Kimmich R. NMR Tomography, Diffusometry, Relaxometry. Berlin: Springer; 1997.
[23] Washburn K, Anderssen E, Vogt S, Seymour J, Birdwell J, Kirkland C, et al. Simultaneous Gaussian and exponential inversion for improved analysis of shales by NMR relaxometry. J Magn Reson 2015;250:7–16.
[24] Mitra P, Sen P, Schwartz L, Le Doussal P. Diffusion propagator as a probe of the structure of porous media. Phys Rev Lett 1992;68:3555–8.
[25] Sen PN. Time-dependent diffusion coefficient as a probe of geometry. Concepts Magn Reson A 2004;23A:1–21.
[27] Ordikhani-Seyedlar A, Stapf S, Mattea C. Dynamics of the ionic liquid 1-butyl-3-methylimidazolium bis(trifluoromethylsulphonyl)imide studied by nuclear magnetic resonance dispersion and diffusion. Phys Chem Chem Phys 2015;17:1653–9.
[28] Carr H, Purcell E. Effects of diffusion on free precession in nuclear magnetic resonance experiments. Phys Rev 1954;94:630–8.
[29] Meiboom S, Gill D. Modified spin-echo method for measuring nuclear relaxation times. Rev Sci Instrum 1958;29:688–91.
[30] Stejskal EO, Tanner JE. Spin diffusion measurements: spin echoes in the presence of a time-dependent field gradient. J Chem Phys 1965;42:288–92.
[31] Blümich B, Perlo J, Casanova F. Mobile single-sided NMR. Prog Nucl Magn Reson Spectrosc 2008;52:197–269.
[32] Tokuda H, Hayamizu K, Ishii K, Susan MdA, Watanabe M. Physicochemical properties and structures of room temperature ionic liquids. 2. Variation of alkyl chain length in imidazolium cation. J Phys Chem B 2005;109:6103–10.
[33] Medved I, Cerny R. Surface diffusion in porous media: a critical review. Microporous Mesoporous Mater 2011;142:405–22.
[34] D'Orazio F, Bhattacharja S, Halperin W. Enhanced self-diffusion of water in restricted geometry. Phys Rev Lett 1989;63:43–6.
[35] Ardelean I, Mattea C, Farrher G, Wonorahardjo S, Kimmich R. Nuclear magnetic resonance study of the vapor phase contribution to diffusion in nanoporous glasses partially filled with water and cyclohexane. J Chem Phys 2003;119:10358–62.
[36] Ma X, Yan L, Wang X, Guo Q, Xia A. Determination of the hydrogen-bonding induced local viscosity enhancement in room temperature ionic liquids via femtosecond time-resolved depleted spontaneous emission. J Phys Chem A 2011;115:7937–47.
[37] Blanco-Díaz E, Vázquez-Montelongo E, Cisneros G, Castrejón-González E. Computational investigation of non-covalent interactions in 1-butyl 3-methylimidazolium bis(trifluoromethylsulfonyl)imide [bmim][Tf2N] in EMD and NEMD. J Chem Phys 2018;148:1–10. (054303).
[38] Dong K, Wang Q, Lu X, Fhou Q, Zhang S. Zhang S, Wang J, Lu X, Zhou Q, editors. Structure, Interaction and Hydrogen Bonds. Chap1. Structures and Interactions of Ionic Liquids. Springer Verlag; 2014.
[39] Fumino K, Wulf A, Ludwig R. Strong, localized, and directional hydrogen bonds fluidize ionic liquids. Angew Chem Int Ed 2008;47:3639–8734.